Hydrogen Bond Networks: Structure and Evolution after Hydrogen Bond Breaking†

John B. Asbury, Tobias Steinel, and M. D. Fayer*

Department of Chemistry, Stanford University, Stanford, California 94305

Received: September 1, 2003; In Final Form: December 18, 2003

The nature of hydrogen bonding networks following hydrogen bond breaking is investigated using vibrational echo correlation spectroscopy of the hydroxyl stretch of methanol-OD (MeOD) of MeOD oligomers in CCl_4. Using ultrafast (<50 fs) infrared multidimensional stimulated vibrational echo correlation spectroscopy with full phase information, the experiments examine frequency correlation between initially excited OD stretches and their "photoproducts" created by hydrogen bond breaking following vibrational relaxation. The hydrogen bond breaking following vibrational relaxation gives rise to a new species, singly hydrogen bonded MeODs, the photoproduct. The photoproducts give rise to a well-defined spectrally distinct off-diagonal peak in the correlation spectrum. Detailed modeling of this peak is used to measure its spectral diffusion (increased spectral broadening as time increases). A rephasing vibrational echo signal and spectral diffusion can only occur if photoproduct hydroxyl stretch frequencies are highly correlated with the frequencies of the initially excited hydroxyl stretches prior to hydrogen bond breaking. The observation of spectral diffusion (fine frequency correlation) demonstrates that broken oligomers have "memory" of initial unbroken oligomers. Possible explanations for the frequency correlation are discussed.

I. Introduction

The hydrogen bonds in liquids such as alcohols and water give rise to hydrogen bonding networks that play a major role in both the structure and dynamics of hydrogen bonding liquids.[1−9] Hydrogen bonds between water or alcohol molecules are relatively weak interactions, and so the hydrogen bonded networks are continually evolving in time.[10] Hydrogen bonds break, and new hydrogen bonds form. Structural evolution causes weak hydrogen bonds to become strong and strong hydrogen bonds to become weak.

Properties of hydrogen bonded networks can be studied using infrared spectroscopy of the hydroxyl stretching mode because of the influence of the number of hydrogen bonds and the strength of hydrogen bonds on the hydroxyl stretch frequency.[11−14] Strong evidence for the correlation between the hydroxyl stretch frequency and the hydrogen bond strength in solids is obtained from correlating crystallographic data and spectroscopic data.[12] Observations on a large number of compounds show that as the hydrogen bond shortens (strengthens) the hydroxyl stretch frequency shifts to the red. The same relationship also applies to liquids.[3,10,11,13,15] In liquids, the widths of the lines, which are caused by inhomogeneous broadening, are attributed to variations in hydrogen bonds strengths and the number and type of hydrogen bond.[10]

The linear absorption spectrum of methanol-OD (MeOD) oligomers in CCl_4 solution is displayed in Figure 1. (In MeOD, a deuterium replaces the hydrogen in the hydroxyl group.) Although methanol is capable of forming up to three hydrogen bonds, one donated and two accepted by the hydroxyl, many MD simulations demonstrate that methanol overwhelmingly forms only two hydrogen bonds, one donated and one accepted, (called δ) whether in the pure liquid[16−19] or as oligomers in CCl_4.[20] δ type MeODs have a very broad hydroxyl stretch band

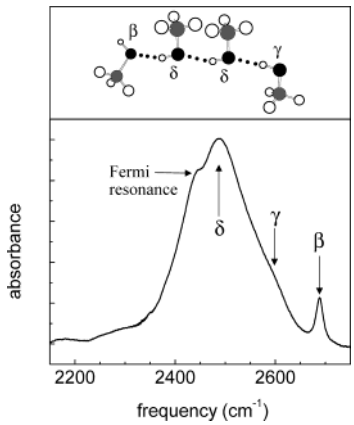

Figure 1. Linear absorption spectrum of a 10% solution of methanol-OD in CCl_4. β's are hydroxyls that are acceptors but not donors. γ's are donors but not acceptors. δ's are both donors and acceptors. These are illustrated schematically at the top of the figure. The shoulder on the red side of the spectrum is a Fermi resonance with the overtone of the methyl rocking mode.

(∼150 cm^{-1}) centered at ∼2490 cm^{-1} (see Figure 1).[15,21−23] There is a shoulder on the red side of the δ band caused by a Fermi resonance with the overtone of the methyl rocking mode.[24] For oligomers that are not rings, each oligomer has two ends that consist of a hydrogen bond donor (called γ) and a hydrogen bond acceptor (called β). For a γ MeOD, the frequency shifts to ∼2600 cm^{-1}, and the spectrum, while still very broad, is significantly narrower than the δ band (∼80 cm^{-1}). A β MeOD absorbs still further to the blue at ∼2690 cm^{-1}, and the band is relatively narrow (∼20 cm^{-1}).[15,21−23] Water also displays spectral shifts to the blue when the extent of hydrogen bonding decreases.[13] However, because water can have many more hydrogen bonds, there is not a simple one-to-one correspondence between the number of hydrogen bonds and the frequency.[13] The description of the structure and evolution of hydrogen bonded networks in methanol is greatly

† Part of the special issue "Hans C. Andersen Festschrift".
* To whom correspondence should be addressed.

10.1021/jp036600c CCC: $27.50
Published on Web 03/20/2004

simplified relative to that in water by the preponderance of doubly hydrogen bonded species. Consequently, methanol oligomers in CCl_4 are an important system for studying the dynamics of hydrogen bonded networks.[25−27]

Although linear-infrared spectroscopy can provide information on the influence of the number and types of hydrogen bonds on the hydroxyl stretch frequency, it cannot be used to examine the evolution of hydrogen bond networks. The time dependence of hydrogen bond strengths causes hydroxyl stretch frequency spectral diffusion.[13] The linear absorption spectrum can only provide time independent information because inhomogeneous broadening of the hydroxyl stretch[7,14,25−33] prevents the spectral evolution from being observed.

It is in the context of hydrogen bond dynamics that ultrafast infrared experiments gain their importance.[7,25−47] Most ultrafast infrared experiments have utilized pump−probe spectroscopy,[7,30,33−36,39−47] which can examine hydroxyl population dynamics. Pump−probe experiments give vibrational lifetimes, hydrogen bond breaking and reformation rates, and some information on spectral diffusion.[7,30,33−36,41,43] The dynamics of hydrogen bond evolution can be explicated with much greater detail using vibrational echo experiments[48−59] because the inhomogeneous contribution to the line shape can be eliminated and the underlying dynamical line shapes can be observed. Because of the complexity of hydrogen bonding systems, analysis of different contributions to dynamical vibrational spectra is enhanced by the use of ultrafast multidimensional methods. Such methods can separate and narrow the dynamic spectral features,[48−59] permitting the observation of various contributions to the dynamics. Multidimensional techniques are beginning to be applied to hydrogen bonding systems.[25−29] Multidimensional stimulated vibrational echo correlation spectroscopy is akin to multidimensional NMR experiments.[60] However, vibrational stimulated echoes operate on a sufficiently fast time scale (tens of fs to ps) to directly examine the time evolution of hydrogen bonding networks.[25−29]

The vibrational echo correlation spectroscopy technique measures the population and vibrational dephasing dynamics in two frequency dimensions, ω_m and ω_τ. The ω_m axis is similar to the frequency axis in frequency resolved pump−probe spectroscopy. The ω_τ axis does not have an analogue in the pump−probe experiment; it provides an additional dimension of information that is contained only in the correlation spectrum. Changes in the peak shapes along the ω_τ axis display the spectral diffusion dynamics.[13,30,61−66] Therefore, vibrational echo correlation spectroscopy separates the vibrational dephasing dynamics from the population dynamics, permitting hydrogen bond dynamics to be extricated with great detail.

Recently, vibrational echo correlation spectroscopy was used to investigate the mechanism of hydrogen bond breaking in MeOD oligomers in CCl_4 following vibrational relaxation of the hydroxyl stretch.[25−27] The shortest mid-IR pulses produced to date (45 fs or 3.4 cycles of light)[25−29] were used to perform the experiments. Because of the very large bandwidth associated with the ultrashort pulses, it was possible to perform experiments on the entire broad hydroxyl stretching 0−1 and 1−2 bands of δ and γ MeODs even though the combined ground state and first excited-state bands are $\sim$400 cm^{-1} wide. The experiments yielded time dependent vibrational echo correlation spectra, which provide information about hydrogen bond dynamics, interactions, and structural evolution that cannot be obtained from other experiments. Detailed calculations of several potential models of hydrogen bond dynamics were used to simulate the correlation spectra. The correlation spectra along with the calculations demonstrated that the hydroxyl's with absorption on the red side of the δ band (strong hydrogen bonds) selectively break hydrogen bonds following vibrational relaxation while the blue side does not.[27] It was proposed that the strong hydrogen bonds (red side of the hydroxyl stretch band) are selectively broken because the low-frequency modes that are excited by vibrational energy relaxation (VER) of the hydroxyl stretch differ from those that are excited by VER of the higher frequency hydroxyl stretches (weaker hydrogen bonds).[27,67] Some results from this previous study will be recapitulated below where necessary.

In the previous report,[27] we did not discuss the spectral diffusion dynamics observed along the ω_τ axis because the hydrogen bond population dynamics under study could be modeled without considering spectral diffusion. In fact, the model calculations assumed that there was no spectral diffusion on the time scale of interest. This paper extends the previous work by investigating the evolution of hydrogen bonded networks through the observation of spectral diffusion following the breaking of hydrogen bonds. The photoproduct γ species that is formed at the point at which the MeOD oligomer breaks reports the structural evolution of the perturbed networks. Using vibrational echo correlation spectroscopy, we focus on the evolution of the off-diagonal photoproduct γ peak along both the ω_m and ω_τ axes. The data demonstrate a coarse correlation along the ω_m axis, which indicates that a δ having strong hydrogen bonds creates a γ photoproduct having a strong hydrogen bond. The data also demonstrate that a fine correlation exists between the initially excited δ and photoproduct γ. The shape of the photoproduct γ peak along the ω_τ axis displays spectral diffusion as the time delay increases, signifying that a memory of the unbroken hydrogen bonded network is preserved in the photoproduct γ despite the large perturbation associated with breaking a hydrogen bond.

II. Experimental Procedures

The experimental methods have been described in detail elsewhere[29] and will be briefly recounted here. The ultrashort IR pulses used for the experiments were generated using a Ti:sapphire regeneratively amplified laser/OPA system. The output of the regen is 26 fs transform limited 2/3 mJ pulses at 1 kHz rep rate. These are used to pump a substantially modified Spectra Physics short pulse IR OPA. The output of the OPA is compressed to produce 45 fs virtually transform limited IR pulses as measured by collinear autocorrelation. For the experiments, the compression was readjusted to give transform limited pulses in the sample as measured by a sample that gave a purely nonresonant signal.

The IR beam is split into 5 beams. Three of the beams are the excitation beams for the stimulated vibrational echo. A fourth beam is the local oscillator (LO) used to heterodyne detect the vibrational echo signal. One of the excitation beams is also used for pump−probe experiments, with the fifth beam as the probe beam in the pump−probe experiments. All of the beams that pass through the sample are optically identical and are compensated for GVD simultaneously. The vibrational echo signal combined with the LO is passed through a monochromator and detected by a 32 element MCT array. At each monochromator setting, the array detects 32 individual wavelengths. Further experimental details have been reported previously.[29]

The sample, 10% MeOD in CCl_4, was held in a sample cell of CaF_2 flats with a spacing of 50 μm. The peak absorbance of the samples was 0.18. Such a low absorbance is necessary to prevent serious distortions of the pulses as they propagate through the sample.

The phase-resolved, heterodyne detected, stimulated vibrational echo was measured as a function of one frequency variable, ω_m, and two time variables, τ and T_w, which are defined as the time between the first and second radiation field-matter interactions and the second and third interactions, respectively. The measured signal is the absolute value squared of the sum of the vibrational echo electric field, S, and the local oscillator electric field, L: $|L+S|^2 = L^2 + 2LS + S^2$. The L^2 term is time-independent and S^2 is negligibly small; hence, neither contributes to the time dependence of the signal. The spectrum of the $2LS$ term is displayed along the ω_m frequency axis. As the τ variable is scanned in 2 fs steps, the phase of the echo electric field is scanned relative to the fixed local oscillator electric field, resulting in an interferogram measured as a function of the τ variable. By numerical Fourier transformation, this interferogram is converted into the frequency variable ω_τ. In NMR, the ω_τ and the ω_m axes are generally referred to as the ω_1 and the ω_3 axes, respectively.

The interferogram contains both the absorptive and dispersive components of the vibrational echo signal. However, two sets of quantum pathways can be measured independently by appropriate time ordering of the pulses in the experiment.[68,69] With pulses 1 and 2 at the time origin, pathway 1 or 2 is obtained by scanning pulse 1 or 2 to negative time, respectively. In principle, by adding the Fourier transforms of the interferograms from the two pathways, the dispersive component cancels leaving only the absorptive component. The 2D vibrational echo correlation spectra are constructed by plotting the amplitude of the absorptive part of the stimulated vibrational echo as a function of both ω_m and ω_τ.

Lack of perfect knowledge of the timing of the pulses and consideration of chirp on the vibrational echo pulse requires a "phasing" procedure to be used.[25,29] The projection slice theorem[29,60,68−70] is employed to generate the absorptive 2D correlation spectrum. The projection of the absorptive 2D correlation spectrum onto the ω_m axis is equivalent to the IR pump−probe spectrum recorded at the same T_w, as long as all of the contributions to the stimulated vibrational echo are absorptive. Consequently, comparison of the projected 2D stimulated vibrational echo spectrum with the pump−probe spectrum permits the correct isolation of the absorptive vibrational echo correlation spectrum from the 2D spectrum obtained from the addition of the two quantum pathways. Details of the phasing procedure including its mathematical formulation have been presented previously.[29] Following phasing, the errors in the time origins are $<100 \times 10^{-18}$ s and the chirp across the entire spectrum is $<100 \times 10^{-18}$ s. The result is accurate correlation spectra from which dynamics can be examined.

III. Results and Discussion

The hydrogen bonded MeOD oligomers studied here are a photochemical system in which vibrational excitation of the hydroxyl stretch results in hydrogen bond breaking.[25−27,30,34−36,71] Recently, vibrational relaxation and hydrogen bond dynamics in MeOD dissolved in CCl_4 were measured with ultrafast infrared pump−probe spectroscopy.[30,34−36,71] The vibrational relaxation lifetime of the δ band is ~500 fs with some wavelength dependence arising from the Fermi resonance with the overtone of the methyl rocking mode[24] (see Figure 1). The studies showed that direct hydrogen bond breaking occurs following vibrational relaxation on a time scale of ~200 fs.[34] The direct hydrogen bond breaking occurs because the excited hydroxyl stretch decays into vibrational modes that lead to the hydrogen bond dissociation.

More recently, an expanded experimental study was presented of vibrational relaxation and hydrogen bond dynamics in MeOD and *d*-MeOD (fully deuterated methanol) dissolved in CCl_4. Frequency resolved IR pump−probe spectra of both molecules were obtained using <50 fs pulses that had a bandwidth spanning the entire δ and γ bands. The appearance of photoproduct γ's was observed as δ's broke hydrogen bonds. In the same study,[27] correlation spectroscopy was used to study both compounds. Quantitative simulations of the correlation spectra were performed for MeOD, and it was determined that hydrogen bonds associated with absorbers on the red side of the δ band, the strongest hydrogen bonds, were selectively broken following vibrational relaxation of the δ MeOD hydroxyl stretch.[27] The comparisons of MeOD and *d*-MeOD experimental results demonstrated that all features of the dynamics of the two systems were the same aside from the MeOD wavelength-dependent lifetime.

A. Correlation Spectra. The general features of the MeOD correlation spectra as a function of T_w have been presented previously.[25−27] They are reviewed here to provide the material necessary for the detailed examination of the dynamical properties of the photoproduct γ band in MeOD that is presented below. The top panel of Figure 2 is a contour plot of the 2D correlation spectra with $T_w = 125$ fs. The contours display equal 10% graduations. The ω_τ axis is the axis of the first matter−radiation field interaction. The ω_m axis is the axis of the emission of the vibrational echo pulse. If the frequency of the first interaction and the emission are the same, a peak will appear on the diagonal. If the frequency of the emission is different from the frequency of the first interaction, a peak will appear off diagonal and be negative going.[72,73] The positive going band on the diagonal corresponds to the 0−1 transition of the δ band with some contribution from the 0−1 γ band on the high-frequency end. The negative going band arises from the 1−2 transition of the δ band. The 1−2 band is off diagonal because the emission is shifted to lower frequency by the vibrational anharmonicity (~150 cm^{-1}).[74] The red edge of the positive going 0−1 band has a contribution from Fermi resonance with overtone of the methyl rocking mode (1232 cm^{-1}).[24] As mentioned above, experiments on fully deuterated methanol, which does not have the Fermi resonance, show that the results presented below are not influenced by the presence of the Fermi resonance in MeOD.[25,27] It should be noted that the shape of the δ 1−2 transition is distorted on the red edge because the laser spectrum falls off rapidly at lower frequency. Consequently, it does not appear elongated along the diagonal like the 0−1 transition. The γ 1−2 transition is not resolved in the correlation spectrum because it is obscured by the much larger δ 0−1 peak.[27]

The lower panels of Figure 2 show contour plots at T_w = 1.2, 1.8, and 5.0 ps for MeOD. At 125 fs the spectrum is dominated by the 0−1 band (positive) and the 1−2 band (negative). By $T_w = 1.2$ ps, the correlation spectrum has changed dramatically. A good fraction of the initially produced excited-state population has decayed to the ground state because the vibrational lifetime of the OD stretch is ~0.5 ps.[34] The magnitude of the δ 1−2 off diagonal peak reflects the δ excited-state decay. Because the lifetime of the γ band (~1 ps) is longer than that of the δ band, the diagonal γ 0−1 band is uncovered as the δ band decays. The γ 1−2 peak is not visible even though its 0−1 transition has been uncovered because the γ 1−2 peak is still buried underneath the remaining δ 0−1 peak. Only the blue side of δ 0−1 band decays completely with the lifetime.[27]

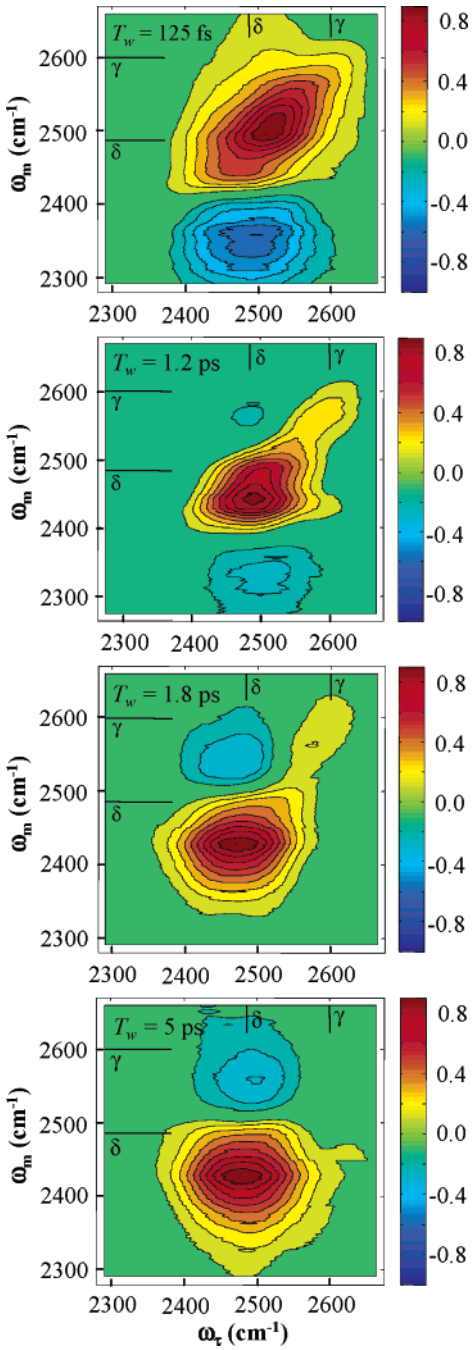

Figure 2. Top panel: the vibrational echo correlation spectrum for $T_w = 125$ fs. The positive going band arises from the 0−1 transition of the hydroxyl stretch. The negative going band arises from the 1−2 transition. Lower panels: contour plots of the correlation spectra for $T_w = 1.2$, 1.8, and 5 ps. As T_w increases, the off-diagonal negative going 1−2 band (bottom) decays, the main band on the diagonal collapses to the red, and a new off-diagonal negative going peak appears at the top of the panel.

Most significant is the appearance of a new off diagonal negative going peak located above the δ band that is beginning to appear at $T_w = 1.2$ ps. As has been shown in detail, this is the photoproduct γ band.[25−27] The peak is off diagonal because the first two radiation field interactions are with the δ band to create an excited state population, but the third interaction is with the newly formed photoproduct γ band created following vibrational relaxation of δ s. The fact that the new band is off diagonal and directly above the contracted δ band helps establish its identity as the photoproduct γ band.

In the 1.8 ps plot, the δ 1−2 peak is gone. The positive going diagonal γ peak is almost gone. The diagonal δ band progressively contracts further to the red as T_w increases. The new off diagonal negative photoproduct γ peak located above the δ band has grown considerably in magnitude. For $T_w = 5.0$ ps, the diagonal γ band is gone. The only remaining features are the red contracted 0−1 δ band and the off diagonal negative going photoproduct γ peak.

Normally, the decay of the excited state into the ground state causes the vibrational echo signal to decay to zero. However, there is both an excited state and ground-state contribution to the signal. Following vibrational relaxation, ∼20% of the initially excited δ's break a hydrogen bond in ∼200 fs, removing them as δ absorbers.[34] Therefore, the decay of the excited state does not completely eliminate the contribution to the signal from the ground state. The ground-state signal remains for the hydrogen bond recombination time, which is tens of ps.[27,34]

Recently, detailed calculations of the correlation spectra displayed in Figure 2 were presented that unambiguously demonstrated that the δ MeOD's with absorption on the red side of the band (strong hydrogen bonds) selectively break hydrogen bonds following vibrational energy relaxation.[27] Here, we recapitulate the principle results of the calculations to provide context for the present discussion of frequency correlation between the hydroxyl stretch of the preserved δ and photoproduct γ distributions. We begin with a brief description of the method for modeling the correlation spectra followed by a presentation of the modeling results. The same modeling method is used in the detailed analysis of the photoproduct γ; therefore, it is discussed in some detail in Appendix I.

B. Modeling Results and Red-Breaking. The vibrational echo correlation spectra were quantitatively simulated by describing them as the sum of overlapping 2-dimensional Gaussian peak shapes, one for each feature in the spectrum.[27] Many of the parameters necessary were obtained from the linear spectrum.[27] The 125 fs spectrum occurs prior to vibrational relaxation and hydrogen bond breaking. After accurately reproducing the 125 fs data, various physical scenarios were tested that could give rise to the later correlation spectra, particularly the 5 ps data. Details of the fitting procedure, which is also used below for examining spectral diffusion, are given in ref 27 and in Appendix I. High quality fits to the correlation spectra have R^2 values (square of the sum of the residuals) of <0.2 (see Appendix I).

The simulation of the $T_w = 5.0$ ps correlation spectrum is displayed in panel b of Figure 3.[27] The data and fit have been normalized to the maximum positive signal. The contours display equal 10% graduations. In the simulation, 5 peaks were included to describe the $T_w = 5$ ps correlation spectrum: the 0−1 transition of the δ band, the 0−1 transition of the γ band, the Fermi resonance peak, and the two cross-peaks between the Fermi resonance and the δ band. The 1−2 transitions of the δ and γ bands (included in the fit to the $T_w = 125$ fs data in ref 27) do not occur in the fit because excited state relaxation completely depletes the excited states of both species by this T_w delay. The R^2 value calculated from eq A3 is 0.13, indicating that the simulated correlation spectrum is a very precise description of the $T_w = 5.0$ ps experimental correlation spectrum. In addition to the main features, the fine features at the center of the δ band are reproduced in the calculation. Panel c displays the projection of the best fit onto the ω_m axis calculated by integrating over the ω_τ axis (see eq A4) compared with the pump−probe spectrum at $T_w = 5$ ps. Note that the ω_m axis is the vertical axis in the 1-dimensional frequency plot. Clearly,

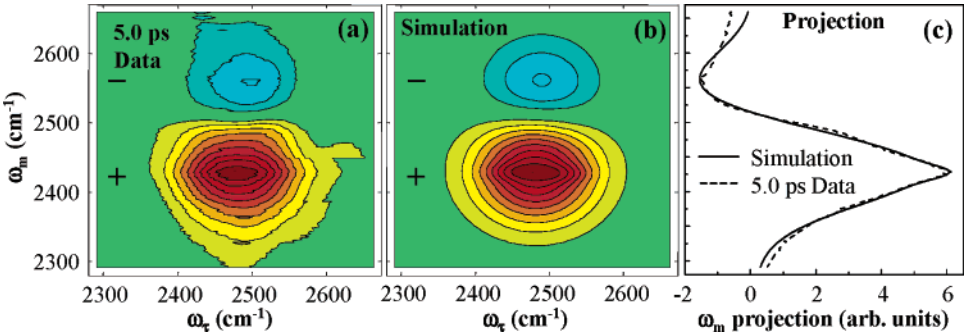

Figure 3. Contour plots of calculated correlation spectrum at 5 ps using the 2-dimensional Gaussian model compared with experimental correlation spectrum. $T_w = 5.0$ ps experimental correlation spectrum (panel a). The calculated correlation spectrum (panel b). The agreement is excellent. Panel c displays the comparison of the projection onto the ω_m axis of the calculated spectrum to the experimental pump−probe data. The fits accurately reproduce the data. Note that the ω_m frequency axis is the vertical axis in panel c, and the horizontal axis displays the peak amplitude integrated over the ω_τ axis. The contours display equal 10% graduations of the normalized data.

the fit is an accurate description of the $T_w = 5$ ps correlation spectrum and pump−probe experimental data. This is in contrast to the other models that were tested in ref 27.

The model used to simulate the $T_w = 5.0$ ps experimental data has been described in detail elsewhere.[27] Only a portion of the δ band was preserved through hydrogen bond breaking. Hence, the preserved bleach and product peaks have different spectra than the δ or γ bands observed in the FTIR spectrum, in contrast with the model used to describe the $T_w = 125$ fs experimental correlation spectrum. The detailed calculations demonstrated that the preserved ground state on the red side of the δ band in the $T_w = 5.0$ ps correlation spectrum can only be described by the model in which the red side of the band breaks hydrogen bonds while the blue side does not.[27] Other models, which assumed that all of the hydrogen bonds in the δ band were either broken or were weakened could not describe the data.[27]

C. Observation of Photoproduct γ Band Spectral Diffusion. Changes in the 2-dimensional photoproduct γ peak shape (spectral diffusion) following hydrogen bond breaking provides information on the structural relationship of the network after hydrogen bond breaking to the network prior to hydrogen bond breaking. The photoproduct γ species are at one end of the oligomer formed by hydrogen bond breaking. The simulated correlation spectra presented above and the detailed analysis presented in ref 27 demonstrate the method's ability to quantitatively describe the vibrational echo correlation spectra. Therefore, we use the same method here to address spectral diffusion dynamics occurring within the photoproduct γ band.

Correlation spectra were measured focusing on the photoproduct γ peak for T_w delays long compared to the excited-state lifetime. Four close-up views of the off-diagonal photoproduct γ peak measured at 3.6, 5.0, 10, and 20 ps T_w delays are displayed in Figure 4 (left column). The out of plane axes, shown as contours in each panel of Figure 4, have been normalized to the absolute value magnitude of the photoproduct γ peak. The contours display equal 10% graduations. For reference, the photoproduct γ peak at the $T_w = 5.0$ ps (Figure 4, panel b, left) is the same as the photoproduct γ peak displayed in the $T_w = 5.0$ ps correlation spectrum shown in Figure 2, except that the scale has been normalized. The amplitude of the photoproduct γ peak decays by a factor of 4 between 3.6 and 20 ps. The decay in the signal is indicated in Figure 4 by the decreased signal-to-noise ratio at longer T_w delay. The photoproduct γ band decays as hydrogen bonds recombine on the ~10 ps time scale.[27,34]

The dynamics of the photoproduct γ peak displayed in Figure 4 reflect only the dynamics of the ground-state hydrogen bonded

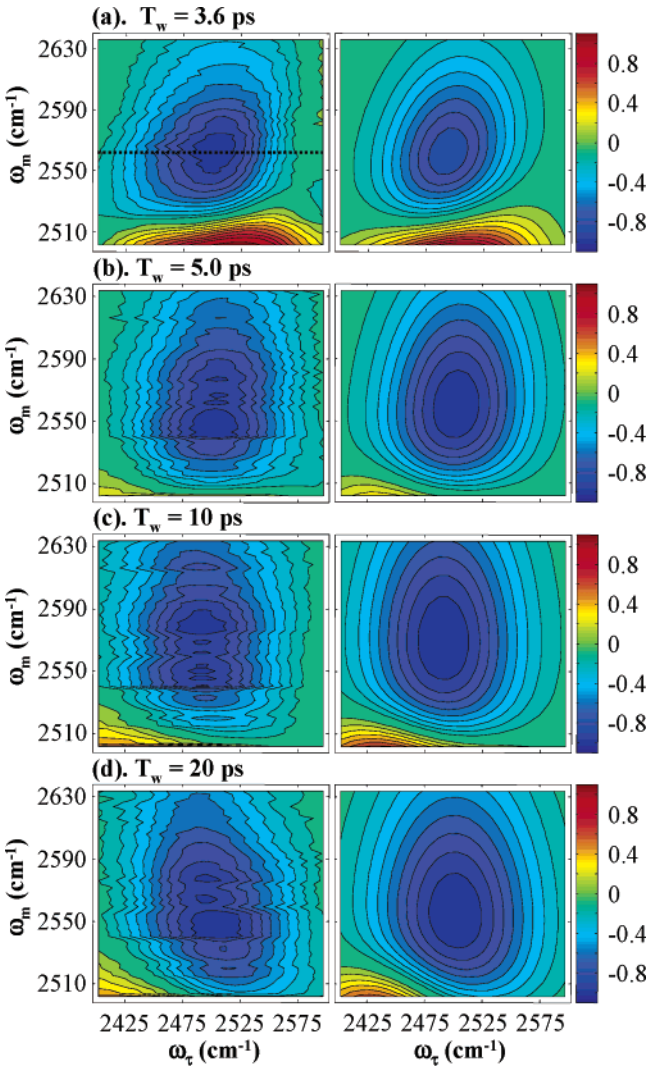

Figure 4. Contour plots of portions of correlation spectra showing the region around the photoproduct γ peak for T_w = (a) 3.6, (b) 5.0, (c) 10.0, and (d) 20.0 ps. The left column shows the experimental data for each T_w delay. The right column shows the fits to the experimental data. As T_w increases, the band shape changes along both the ω_m and ω_τ axes. The broadening along the ω_m axis results from the evolution toward the equilibrium spectrum of the initially prepared photoproduct γ distribution. Spectral diffusion along the ω_τ axis reports the dephasing dynamics of the photoproduct γ peak.

network because the excited-state dynamics are complete (δ and γ vibrational lifetimes 0.5 and 1 ps, respectively). At $T_w = 3.6$ ps, the photoproduct γ peak is narrowest along both ω_m and ω_τ

axes. As T_w increases, the peak shows the influence of equilibration of the perturbed hydrogen bond network and spectral diffusion dynamics. As T_w increases, the initially created photoproduct γ spectral distribution, which is narrowed and red shifted along the ω_m axis, equilibrates to its steady-state distribution, which increases the width of the peak along the ω_m axis. Spectral diffusion results in the increase of the dynamical line width along the ω_τ axis as T_w increases.

From the model previously used to simulate the $T_w = 5.0$ ps experimental data (see Figure 3, panel b), we assigned a center frequency of 2560 cm^{-1} to the photoproduct γ peak.[27] The apparent center of the photoproduct γ peak displayed in Figures 2−4 confirms this assignment (note the displacement along the ω_m axis of the photoproduct γ peak from the horizontal line that marks the center frequency of the equilibrium γ peak in Figure 2). The photoproduct γ band is red shifted by about 40 cm^{-1} relative to the initially excited γ distribution. This frequency shift indicates the photoproduct γ's are not randomly distributed throughout the inhomogeneous γ band but are created with at least some frequency correlation with their origin on the low-frequency side of the δ band.

The correlation spectra displayed in Figures 2−4 contain the dynamical line shape along the ω_τ axis as a function of frequency and waiting time, T_w. Changes in the dynamical line shape as a function of T_w give the spectral diffusion dynamics occurring within the hydroxyl stretch peak.[13,30,61−66]

The qualitative changes in the dynamical line shape can be seen in the data by looking at a cross sectional cut of the photoproduct γ peak at a particular ω_m value and projecting it onto the ω_τ axis. The horizontal dashed line shown in the $T_w = 3.6$ ps panel of Figure 4 (panel a, left) illustrates such a cut at the apparent center of the photoproduct γ hydroxyl stretch peak at ∼2560 cm^{-1}. As T_w increases, the photoproduct γ band changes shape and the ∼2560 cm^{-1} cut becomes broader. The dynamical line measured in the correlation spectra is narrow when spectral diffusion has not randomized the distribution of hydroxyl stretch frequencies. As spectral diffusion occurs, the dynamical line width broadens. Because the hydroxyl stretch frequency is correlated with the strength of hydrogen bonds,[3,10−15] the time evolution of the vibrational echo correlation spectra reflects the structural evolution of the hydrogen bonding network.

To quantify the spectral diffusion dynamics observed in the photoproduct γ peak as a function of T_w delay, we simulated the correlation spectra displayed in Figure 4 using the model described above and in Appendix I. One 2-dimensional Gaussian peak was used to describe the photoproduct γ band, and another was used for the preserved δ band, which appears as the positive going feature barely visible at the bottom of the correlation spectra in Figure 4 and can be seen in Figures 2 and 3. Although the δ band is not shown in detail in Figure 4, its inclusion in the calculations is necessary to obtain a correct description of the γ band. The Fermi resonance peak and its two cross-peaks with the δ band were included as well. Their positions and amplitudes relative to the preserved δ bleach were determined from the fit to the $T_w = 125$ fs correlation spectrum.[27]

The right column of Figure 4 displays the corresponding 2-dimensional Gaussian fit to each correlation spectrum at $T_w = 3.6$, 5.0, 10, and 20 ps. The 2-dimensional Gaussian fitting procedure enables us to quantitatively measure the dynamical line width of the photoproduct γ peak without interference from the preserved δ peak or the three peaks associated with the Fermi resonance. After fitting the correlation spectra, the amplitudes of every peak except the photoproduct γ peak are nulled. A cross sectional cut of the photoproduct γ peak at $\omega_m = 2560$ cm^{-1} is fit with a Gaussian. The resulting fwhm is a measure of the dynamical line width. Figure 5 displays the dynamical line widths extracted from the vibrational echo correlation spectra displayed in Figure 4 plotted versus the corresponding T_w delay. The error bars indicate the upper and lower bounds of the fit to the dynamical line width at which the R^2 values (see eq A3 Appendix I) are twice there optimal value. The line through the data is a guide to the eye. At the shortest T_w delay following the completion of vibrational relaxation ($T_w = 3.6$ ps), the dynamical line width is ∼90 cm^{-1}. This width grows to ∼120 cm^{-1} by $T_w = 20$ ps. The 2-dimensional Gaussian fitting procedure captures other aspects of the evolution of the shape of the photoproduct γ peak with increasing T_w delay. The correlation spectra measured at $T_w = 3.6$ and 5.0 ps display a slight tilt along the diagonal, which is a characteristic of inhomogeneous broadening.[65,66] The tilted shape is reproduced by the fit because we modeled the peaks with 2-dimensional Gaussian shapes that were elongated along the diagonal. The slight tilt indicates that spectral diffusion has not completely randomized the frequencies in the photoproduct γ hydroxyl stretch by $T_w = 5.0$ ps, which is consistent with the changing dynamical line width displayed in Figure 5. The photoproduct γ peak is slightly elongated along the diagonal in the $T_w = 10$ and 20 ps correlation spectra as well. However, the elongation is obscured in the data displayed by the presence of the Fermi resonance cross-peak that appears around ($\omega_m \sim 2490$ cm^{-1}, $\omega_\tau \sim 2430$ cm^{-1}), which results in the positive going signal at the lower left of the correlation spectra (see Figure 4).

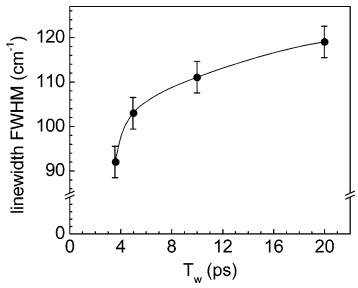

Figure 5. Plot of the fwhm of photoproduct γ peak along the ω_τ axis versus T_w. Changes in the dynamical line width are direct evidence of spectral diffusion. Spectral diffusion along the ω_τ axis demonstrates the existence of fine frequency correlation in the photoproduct γ band (see Figure 6). The line through the data is a guide to the eye.

The photoproduct γ peak also broadens along the ω_m axis as T_w increases, (see Figure 4). The fwhm of the fit to the photoproduct γ peak measured along the ω_m axis increases from ∼120 cm^{-1} at 3.6 ps to ∼180 cm^{-1} at 20 ps as the initially created photoproduct γ spectral distribution equilibrates to the steady-state distribution. This equilibration is visible along the ω_m axis because only a subset of the inhomogeneous γ distribution is created by hydrogen bond breaking. This subset will eventually randomize and sample the full configuration space available to the photoproduct γ MeOD s.

D. Frequency Correlation. Above, we have shown that the photoproduct γ band displays spectral diffusion. Furthermore, the photoproduct γ band is initially created shifted to the red relative to the equilibrium γ band. The shift of the photoproduct γ band to the red shows that there is at least some frequency correlation between the parent δ's and the photoproduct γ's, which we call *coarse correlation*. By coarse correlation, we mean that a δ having two stronger than average hydrogen bonds produces a photoproduct γ having one stronger than average hydrogen bond. That this correlation must exist can be

understood in the following way. If there were no frequency correlation between the parent δ's and the photoproduct γ's, the photoproduct γ's would have a center frequency and line width along the ω_m axis that is identical to the equilibrium γ band. Without correlation, the photoproduct γ's could be anywhere in the γ line with a probability weighted only by the line shape. The red sides of the δ and γ bands correspond to stronger hydrogen bonds than average.[3,10−15] Therefore, breaking the stronger hydrogen bonds in the δ band gives rise to a photoproduct γ band composed of γ's with stronger hydrogen bonds. At long time, the γ frequencies will randomize throughout the equilibrium γ band and, therefore, throughout the full range of hydrogen bond strengths. This is observed as the spreading of the photoproduct γ band along the ω_m axis.

The data also demonstrate that there is a more subtle type of correlation that we call fine *frequency correlation*. The fine correlation shows that a direct correlation exists between a δ absorber at frequency ω_0 and a narrow distribution of photoproduct γs centered at frequency $\omega_0 + \Delta$, where $\Delta = \sim 130$ cm^{-1} [27] is the shift in the hydroxyl stretch frequency that results from breaking a hydrogen bond. Fine frequency correlation will occur if the photoproducts have a detailed "memory" of the structure of the prior intact hydrogen bonded networks, which is slowly erased as the broken networks evolve in time away from their structures immediately following hydrogen bond breaking.

To elaborate on how the microscopic situation of coarse and fine correlation affects the experimental observables, it is necessary to consider the types of influences the light pulse sequence can have on the sample. There are two types of radiation field/matter quantum pathways that can give rise to the photoproduct γ signal, which display different behavior in the vibrational echo correlation spectra. These pathways can be represented diagrammatically.[72] One contribution to a vibrational echo signal can come from nonrephasing grating diagrams[72] that produce a signal only when pulses 1 and 2 are within the free induction decay (FID) time of each other. When pulses 1 and 2 are within the free induction decay time of each other, there is interference between the electric field of the second pulse and the polarization induced in the sample by the first pulse. The polarization decays with the FID and results in the requirement that the two pulses must be within the FID. The interference gives rise to optical fringes, that is, alternating spatial regions of light and dark in the sample. Excited states are only produced in the light regions. The alternating regions of excited states and no excited states give rise to excited state and ground-state population diffraction gratings. Relaxation to the ground state followed by hydrogen bond breaking will preserve the ground state *population grating* (one of the nonrephasing grating diagrams) and create a photoproduct γ population grating in place of the excited-state population grating. The third pulse in the vibrational echo sequence can diffract from a population grating to produce a signal in the vibrational echo phase matched direction. For a fixed T_w, as τ is scanned, the population grating (nonrephasing) signal will decay with the free induction decay time of the entire initially excited δ band. This is an important point. The FID that determines whether a population grating is formed follows the first pulse that excites the entire δ band prior to vibrational relaxation and hydrogen bond breaking. The second important point is that as τ is scanned the signal decays, but its decay is independent of T_w because it is determined solely by the δ FID. The dynamical line width is also independent of T_w because it is the Fourier transform of the δ FID.

There is a second set of diagrams, rephasing diagrams, that give rise to a true vibrational echo signal.[72] These can be viewed physically in terms of a variation in population as a function of frequency, a *frequency grating*. Following the second pulse, frequency fringes are produced, that is, alternating frequency regions of excited states and ground states. At a frequency where there is an excited state peak, there is a corresponding ground state hole. Relaxation to the ground state followed by hydrogen bond breaking will eliminate the excited state peaks but not completely fill in the ground-state holes, preserving the ground state *frequency grating* in the δ band. If and only if there is fine frequency correlation will a frequency grating be created in the photoproduct γ band. If there is fine frequency correlation, the third pulse in the vibrational echo sequence triggers a rephasing process that gives rise to the vibrational echo signal at both the δ and photoproduct γ transition frequencies.

The importance of the rephasing diagrams to elucidating hydrogen bond dynamics can be understood in the following way. The *frequency grating* written into the hydroxyl stretch band sub-divides the inhomogeneous distribution of hydrogen bond strengths by leaving some MeOD's in the vibrational excited state and others in the ground state, depending upon their frequency. The frequency dependent (and hence structure dependent) pattern of excited and grounds states in the initially excited δ band permits each sub-ensemble within the inhomogeneous distribution to be probed independently. As time progresses, the structures of the hydrogen bonded networks evolve and the vibrational frequency of a particular δ in the network changes, resulting in spectral diffusion. As the T_w delay increases, the hydrogen bond networks evolve and the resulting spectral diffusion causes the rephasing signal to decay faster as τ is scanned. The Fourier transform of the τ scan is the dynamic line width (a cut along the ω_m axis projected onto the ω_τ axis). Therefore, changes in the dynamical line width display the spectral diffusion dynamics and report the evolution in the structure of the hydrogen bonded networks (see Figure 5). Following vibrational relaxation, hydrogen bond breaking preserves part of the ground state δ frequency grating and creates photoproduct γs. If fine frequency correlation exists, the photoproduct γ band will also consist of a ground-state frequency grating, and it will display broadening of its dynamic line width, which is indicative of spectral diffusion.

If only the nonrephasing diagrams contribute to the photoproduct γ signal, then coarse frequency correlation may be observed, but the dynamical line width will be independent of T_w. No spectral diffusion and no fine frequency correlation will be observed. However, if the rephasing diagrams contribute to the photoproduct γ signal, then both coarse and fine frequency correlation can be observed. In this case, the dynamical line width of the photoproduct γ band will increase with increasing T_w, displaying the spectral diffusion dynamics, and hence the structural evolution of the photoproduct γ band hydrogen bonded network. Spectral diffusion in the photoproduct γ band is observed as displayed in Figures 4 and 5.

The two scenarios introduced above are displayed schematically in Figure 6 to illustrate the connection between the nonrephasing and rephasing pathways and the coarse and fine frequency correlation. Panel 1 presents a heuristic display of the spectra of the δ and γ species (dashed lines) that are initially excited (note, the relative amplitudes have been normalized for clarity). δ's with stronger than average hydrogen bonds preferentially break a hydrogen bond, which prevents excited-state relaxation from depleting the ground-state bleach and preserves a subset of the δ distribution on the red side of the δ

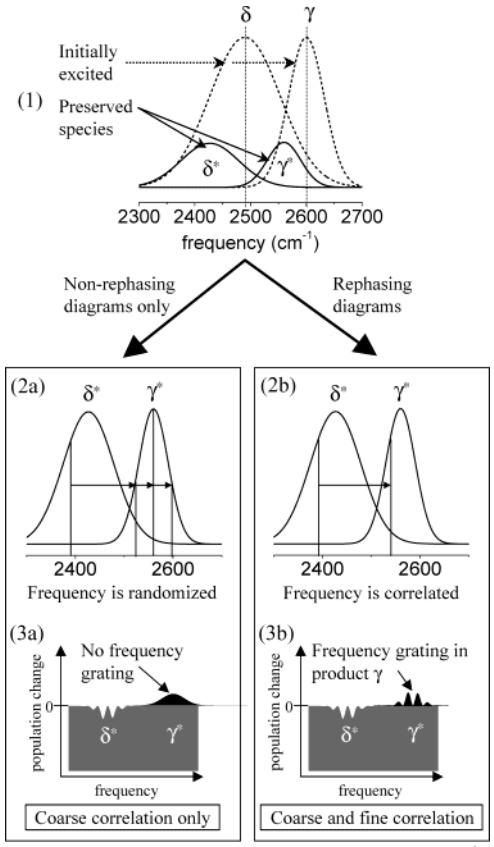

Figure 6. Schematic illustration connecting the influence of the nonrephasing and rephasing pathways to the experimentally observed coarse and fine frequency correlation between the δ and photoproduct γ bands. Panel (1): Coarse frequency correlation is observed between δ's and photoproduct γ's because the species preserved through hydrogen bond breaking are spectrally distinct from the initially excited species. Left column: Only the nonrephasing diagrams contribute to the photoproduct γ signal. Coarse frequency correlation is observed, but the frequency of a particular δ absorber is randomized within the photoproduct γ distribution (see panel 2a). No spectral diffusion is observed in the photoproduct γ signal because no frequency grating was transferred (see panel 3a). Right column: The rephasing diagrams contribute to the photoproduct γ signal. Coarse and fine frequency correlation are observed because the frequency of a particular δ absorber is *not* randomized within the photoproduct γ distribution (see panel 2b). The frequency grating from the initially excited δ distribution is transferred to the photoproduct γ distribution (see panel 3b) and spectral diffusion is observed.

band.[27] The preserved subset, labeled δ* in Figure 6, appears on the low-frequency side of the δ band (solid line). The products of the δ subset that broke a hydrogen bond are the photoproduct γ's, labeled γ* in Figure 6. They retain some memory of their origin, also appearing on the low-frequency side of the γ band as the solid line. The shift of the δ* and γ* spectra relative to the initially excited δ and γ spectra indicates the coarse frequency correlation that exists between the two species. The left column of Figure 6 illustrates the situation in which only the nonrephasing diagrams contribute to the photoproduct γ signal. In this case, (see panel 2a) the frequency of a particular subset of δ absorbers within the δ* distribution (represented by the solid vertical line under the δ* peak) is uncorrelated in frequency with any particular subset of photoproduct γ absorbers within the γ* distribution. Although the frequencies of the δ* and γ* species are coarsely correlated, the frequency of a particular δ absorber that broke a hydrogen bond is randomized within the restricted photoproduct γ distribution. Therefore, no frequency grating is transferred to the photoproduct γ band (see panel 3a). In this situation, the dynamical line width would be independent of T_w and no spectral diffusion dynamics could be observed.

The experimental data clearly demonstrate that the photoproduct γ signal observed in the correlation spectra displayed in Figures 2−4 cannot be described by the nonrephasing diagrams because the dynamical line widths displayed in Figure 5 increase with increasing T_w. The rephasing diagrams must also contribute to the photoproduct γ signal. This situation is illustrated in the right column of Figure 6. For rephasing diagrams to contribute to the photoproduct γ signal, a particular subset of δ absorbers within the δ* distribution must be correlated in frequency with a particular subset of photoproduct γ absorbers within the γ* distribution (represented by the solid vertical line under the γ* peak, see panel 2b). As a result of this fine frequency correlation, the frequency grating written into the initially excited δ distribution is transferred to the photoproduct γ distribution (see panel 3b). The frequency grating in the photoproduct γ distribution sub-divides the distribution and enables the sub-ensembles (different hydrogen bonded structures) to be probed independently, which narrows the dynamical line width measured in the correlation spectra. Structural evolution of the hydrogen bond networks randomizes the frequencies within the photoproduct γ band and results in spectral diffusion, which broadens the dynamical line width. Therefore, the increasing dynamical line width displayed in Figure 5 demonstrates that both coarse and fine frequency correlation exist between the δ and photoproduct γ species because aspects of the structure of the hydrogen bonded network are preserved through hydrogen bond breaking.

E. Mechanisms for Frequency Correlation. The observation of fine frequency correlation means that the photoproduct γ's have memory of the frequency of the original unbroken oligomer. A γ is the end of the oligomer piece that was created by breaking a hydrogen bond in the original oligomer. Because the hydroxyl stretch frequency is correlated with structure, memory of the frequency implies memory of the original structure that gave rise to the new oligomer fragment. Here we will consider two likely mechanisms that could give rise to the frequency memory. In the first mechanism, the two hydrogen bonds associated with a δ MeOD are correlated in strength and therefore the hydroxyl stretches of neighboring δ MeODs are correlated in frequency. Frequency correlation is transferred from the initially excited δ to the photoproduct γ through this correlation. In the second mechanism, the two hydrogen bonds are not correlated in strength. However, when a hydrogen bond breaks, the resulting γ MeOD retains memory of the initially excited hydrogen bond through other structural degrees of freedom that make up the local environment and in part determine the frequency.

The first mechanism involves the correlation of the strengths of adjacent hydrogen bonds. The strength of a hydrogen bond is correlated to its length,[3,10−15] although the angle and donating hydroxyl bond length can have significant influence as well.[13,75,76] Therefore, the first mechanism involves correlation in the microscopic density variations across the hydrogen bonded network that extend over one or more MeODs. When a stronger than average hydrogen bond in a high microscopic density region of the network is excited and subsequently breaks, the remaining adjacent hydrogen bond, which produces the γ, is also a stronger than average hydrogen bond. If the hydrogen bond strength is the overwhelming factor that determines the frequency, then the frequency of the photoproduct γ will be correlated with the reactant δ, consistent with the observations.

There is some data that suggests correlation between the two hydrogen bonds of δ MeODs from the linear absorption spectrum and the correlation spectra. When an α MeOD (a monomer that exists at very low concentration in CCl_4) accepts a hydrogen bond, it becomes a β MeOD.[24,34,35] The resulting shift in the hydroxyl frequency is too small to be observed at room temperature. This demonstrates that accepting a hydrogen bond does not significantly influence the hydroxyl stretch frequency. When a γ MeOD accepts a hydrogen bond, it becomes a δ MeOD. The hydroxyl frequency shift when a γ becomes a δ is $\sim$100 cm^{-1}. This shift must be due to the influence of accepting a hydrogen bond on the strength of the donated hydrogen bond because of the lack of a shift between an α and a β.

It is possible that this gross affect occurs at a finer level. In the network, if a stronger acceptor produces a stronger donor that produces a strong accepting neighbor, there could be local hydrogen bond strength correlation in the network and, therefore, frequency correlation. The correlation spectra at long time in Figures 2−4 show that the red contracted δ gives rise to a red contracted γ. Thus, there is at least coarse frequency correlation of this type. When the δ MeOD breaks a hydrogen bond and the photoproduct γ is produced, the structural degrees of freedom that preserve the hydrogen bond of the photoproduct γ cannot change instantaneously. Therefore, the photoproduct γ will be formed with frequency correlation that is then lost by structural evolution of the fragmented network, which gives rise to spectral diffusion in the photoproduct γ band.

The second mechanism recognizes that other structural degrees of freedom besides the donated and accepted hydrogen bonds may contribute to the δ and γ hydroxyl stretch transition frequencies. In MeOD, there are the positions and orientations of the methyl groups, as well as the configuration of other MeOD's that are not directly hydrogen bonded to the MeOD of interest. For the oligomers studied here in CCl_4, there is also the local solvent configuration. In pure MeOD, the surrounding liquid that is not directly hydrogen bonded to an initially excited δ could be considered the solvent. When the reactant δ is broken and the photoproduct γ is formed, the other degrees of freedom of the oligomer and the solvent will not necessarily be affected immediately. Preservation of these other structural degrees of freedom could produce the observed frequency correlation.

The photoproduct γ peak appears red shifted 40 cm^{-1} relative to the γ band in the linear absorption spectrum. This red shift is a significant fraction of the total shift caused by the second hydrogen bond ($\sim$100 cm^{-1}). Therefore, the gross memory of the broken hydrogen bond must be comparatively strong relative to the hydrogen bond that was initially present. It is questionable whether the local environment can play a strong enough role in determining the hydroxyl stretch frequency to produce this type of coarse frequency correlation. However, the demonstrated existence of a frequency grating in the red contracted photoproduct γ band requires a fine as well as coarse frequency memory.

The existence of both coarse and fine frequency correlation may be consistent with both mechanisms contributing to the frequency correlation exhibited by the γ photoproduct, which suggests the following physical picture. For a given hydrogen bonded oligomer of MeOD's, the strengths of adjacent hydrogen bonds are correlated and the microscopic density of the network is higher in places due to the shorter hydrogen bonds that connect two or more MeOD's. When a hydrogen bond breaks and a δ becomes a γ, the microscopic density in the network cannot immediately respond to the perturbation, which produces the coarse frequency correlation observed along the ω_m axis. In addition, other structural degrees of freedom of the network are not immediately randomized, which produces the fine frequency correlation. As the T_w delay increases, the perturbed network evolves away from its initial structure. The microscopic density changes around the photoproduct γ, which causes the spectral evolution observed along the ω_m axis as T_w increases. The other degrees of freedom of the network and the solvent also randomize, which erases the fine frequency correlation and causes the dynamical line width to increase along the ω_τ axis.

The fine and coarse frequency correlation described in this paper further supports the model of hydrogen bond dynamics presented previously[27] in which it was shown that the strongest hydrogen bonds are selectively broken giving rise to the photoproduct γ band (see Figure 3 and the discussion surrounding it). Another mechanism, in which energy is deposited into the networks by vibrational relaxation causing all of the hydrogen bonds to weaken is inconsistent with fine frequency correlation. The fine frequency correlation in particular as well as the coarse frequency correlation demonstrates that the hydrogen bond network around the photoproduct γ retains significant memory of the prior unbroken network. If vibrational relaxation resulted in "heating" of the network and, therefore, weakening of all of the hydrogen bonds, then there could be no fine frequency correlation. Changing the frequency of every hydrogen bond and, thus, every hydroxyl stretch cannot result in a correlation with the selected set of hydroxyl stretches that composed the initial excited state frequency grating. Therefore, a heating mechanism can be ruled out as the source of the data displayed in Figures 2 and 3. At sufficiently long times (many 10s of ps) pump−probe experiments have shown that there is a heat induced shift in the equilibrium number of hydrogen bonds.[34,35] However, this heating effect is distinct from the observations discussed here and in ref 27.

IV. Concluding Remarks

Vibrational echo correlation spectroscopy has been used to examine details of the hydrogen bonding system, methanol-OD in CCl_4. Structural aspects of hydrogen bonded networks were explicated by observing the evolution of the networks after they were perturbed by hydrogen bond breaking. It was determined that hydrogen bond breaking following vibrational relaxation of a hydroxyl stretch produces a photoproduct with frequency "memory" of the parent network.

At short time, the correlation spectrum (see Figure 2, top panel) is dominated by the hydrogen bonded OD stretch 0−1 transition (positive going peak) and the 1−2 transition (negative going peak). The stimulated vibrational echo signal can be observed for times long compared to the vibrational lifetime ($\sim$500 fs) because of the breaking of hydrogen bonds. As shown in Figure 2 in the lower panels, as T_w is increased beyond the vibrational lifetime, the broad diagonal δ band (MeODs that are hydrogen bond donors and acceptors) contracts to the red side of the line because of selective breaking of the stronger hydrogen bonds (red side of the absorption line). As the hydrogen bonds break, the off-diagonal photoproduct γ (hydrogen bond donor but not acceptor) band grows in.

The data demonstrate that the hydroxyl's with absorption on the red side of the δ band (strong hydrogen bonds) create a photoproduct γ band that is frequency correlated with the initially excited δ band. The photoproduct γ band is created on the red side of the equilibrium γ inhomogeneous distribution. The red shifted spectrum of the photoproduct γ shows that there is coarse frequency correlation between the reactant δ's and

the photoproduct γ's. As time progresses, the photoproduct γ band broadens along the ω_m axis. Spectral evolution along the ω_m axis, which can be observed in a frequency resolved pump−probe experiment, cannot discriminate between coarse frequency correlation (see Figure 6, left column) and fine frequency correlation (see Figure 6, right column) in the generation of the photoproduct γ's. However, the time dependent correlation spectra provide a second frequency axis, the ω_τ axis. Spectral diffusion is observed along the ω_τ axis (see Figures 4 and 5). The observation of spectral diffusion shows that the frequency grating created in the δ excited state by the application of the first two excitation pulses is transferred, at least to some extent, to the photoproduct γ band by hydrogen bond breaking. Therefore, there is fine frequency correlation in the photoproduct γ band. The frequencies are not randomized by hydrogen bond breaking. Therefore, there is structural memory of the parent hydrogen bonded oligomer by the oligomer fragment formed by hydrogen bond breaking

Acknowledgment. This work was supported by the Air Force Office of Scientific Research (Grant No. F49620-01-1-0018), with additional support provided by the Department of Energy (Grant DE-FG03-84ER13251), and the National Science Foundation (DMR-0332692). T.S. thanks the Emmy Noether program of the DFG for partial support.

Appendix I: Method for Modeling the Correlation Spectra

The vibrational echo correlation spectra were quantitatively simulated by describing them as the sum of overlapping 2-dimensional Gaussian peak shapes having the following form[27]

$$S(\omega_m,\omega_\tau) = \sum_i [A_i \exp(-(\cos(\theta)(\omega_m - \omega_{m,i}) + \sin(\theta)(\omega_\tau - \omega_{\tau,i}))^2/2\sigma_{d,i}{}^2) \exp(-(\sin(\theta)(\omega_{m,i} - \omega_m) + \cos(\theta)(\omega_\tau - \omega_{\tau,i}))^2/2\sigma_{a,i}{}^2)] \quad \text{(A1)}$$

The summation is over all 2-dimensional peaks that contribute to the correlation spectrum. The parameters A_i describe the amplitudes of the 2-dimensional peaks. The terms including the angle θ reflect a 45° coordinate transformation from the (ω_m,ω_τ) plane to the (ω_d,ω_a) plane (the plane constructed from the diagonal and anti-diagonal axes). This transformation allows the diagonally elongated peak shapes to be described by a simple 2-dimensional Gaussian function. The positions $\omega_{m,i}$ and $\omega_{\tau,i}$ reflect the position of the ith peak in the (ω_m,ω_τ) plane. The widths of the peaks along the diagonal and anti-diagonal are represented by $\sigma_{d,i}$ and $\sigma_{a,i}$, respectively. The diagonal and anti-diagonal widths for the ith peak are constrained to produce a total line width equal to the corresponding linear line width, fwhm_i, which we obtain by fitting the FTIR spectrum of the sample (see Figure 1).[27] The constraint is enforced in the fitting procedure by the following relationship between $\sigma_{d,i}$, $\sigma_{a,i}$ and fwhm_i

$$\sigma_{a,i} = \{[(\text{fwhm}_i/2.35)^2 - (\sin(\theta))^2\sigma_{d,i}{}^2]/(\cos(\theta))^2\}^{1/2} \quad \text{(A2)}$$

Consequently, for each peak, only one independently adjustable parameter is used to determine the 2-dimensional shape of the peak. The only exception is the 1−2 transition of the δ band in the $T_w = 125$ fs correlation spectrum. This peak shape is distorted by the red edge of the laser spectrum. Consequently, this highly constrained model was not used to fit this peak. The full width at half-maximum of the Fermi resonance and its cross-peaks with the δ band are determined from a best fit to the $T_w = 125$ fs correlation spectrum (see Figure 4, top row).

The best fits to the correlation spectra are obtained by minimizing the integral over the square of the residual volume[27]

$$R^2 = 100 \frac{\int\int (S_{Corr}(\omega_m,\omega_\tau) - S_{Fit}(\omega_m,\omega_\tau))^2 \text{abs}(S_{Corr}(\omega_m,\omega_\tau))\, d\omega_t\, d\omega_m}{\int\int \text{abs}(S_{Corr}(\omega_m,\omega_\tau))^3\, d\omega_t\, d\omega_m} \quad \text{(A3)}$$

resulting from subtracting the 2-dimensional Gaussian fit, $S_{Fit}(\omega_m,\omega_\tau)$, from the experimental correlation spectrum, $S_{Corr}(\omega_m,\omega_\tau)$. The residual volume is weighted by the absolute magnitude amplitude of the correlation spectrum and normalized by the total volume raised to the appropriate power. This evaluation scheme emphasizes the peaks in the correlation spectrum over the wings and the area containing no signal. Much of the area in the 2-dimensional frequency map contains no signal. Small amounts of noise in these areas can grow to dominate the sum of the squares of the residuals due to the large area over which they are integrated. This problem is avoided by weighting the residuals according to eq A3.

The fitting procedure uses two complimentary experiments to constrain the best fit of the 2-dimensional correlation spectra, the linear absorption spectrum (see Figure 1) and the IR pump−probe spectra (not shown). The calculated 2-dimensional fit is projected onto the ω_m axis by integrating over the ω_τ axis to calculate the pump−probe spectrum, $S_P(\omega_m)$, corresponding to the fit[27]

$$S_p(\omega_m) = \int S_{fit}(\omega_m,\omega_\tau)\, d\omega_\tau \quad \text{(A4)}$$

The 2-dimensional fit is constrained to reproduce the IR pump−probe spectrum when projected onto the ω_m axis. High quality fits to the correlation spectra have R^2 values of <0.2 (see eq A3).

References and Notes

(1) Choppin, G. R. *J. Mol. Struct.* **1978**, *45*, 39.
(2) Dore, J. C. *J. Mol. Struct.* **1991**, *250*, 193.
(3) Falk, M.; Ford, T. A. *Can. J. Chem.* **1966**, *44*, 1699.
(4) Luck, W. A. P. *Intermol. Forces* **1991**, 217.
(5) Ludwig, R. *Angew. Chem., Int. Ed.* **2001**, *40*, 1808.
(6) Bakker, H. J.; Woutersen, S.; Nienhuys, H. K. *Chem. Phys.* **2000**, *258*, 233.
(7) Gale, G. M.; Gallot, G.; Hache, F.; Lascoux, N.; Bratos, S.; Leicknam, J. C. *Phys. Rev. Lett.* **1999**, *82*, 1068.
(8) Lawrence, C. P.; Skinner, J. L. *Chem. Phys. Lett.* **2003**, *369*, 472.
(9) Woutersen, S.; Emmerichs, U.; Nienhuys, H.-K.; Bakker, H. J. *Phys. Rev. Lett.* **1998**, *81*, 1106.
(10) Pimentel, G. C.; McClellan, A. L. *The Hydrogen Bond*; W. H. Freeman and Co.: San Francisco, CA, 1960.
(11) Mikenda, W. *J. Mol. Struct.* **1986**, *147*, 1.
(12) Novak, A. Hydrogen bonding in solids. In *Structure and Bonding*; Dunitz, J. D., Ed.; Springer-Verlag: Berlin, 1974; Vol. 18, p 177.
(13) Lawrence, C. P.; Skinner, J. L. *J. Chem. Phys.* **2003**, *118*, 264.
(14) Lawrence, C. P.; Skinner, J. L. *J. Chem. Phys.* **2002**, *117*, 8847.
(15) Liddel, U.; Becker, E. D. *Spectrochim. Acta* **1957**, *10*, 70.
(16) Haughney, M.; Ferrario, M.; McDonald, I. R. *J. Phys. Chem.* **1987**, *91*, 4934.
(17) Matsumoto, M.; Gubbins, K. E. *J. Chem. Phys.* **1990**, *93*, 1981.
(18) Marti, J.; Padro, J. A.; Guardia, E. *J. Mol. Liq.* **1995**, *64*, 1.
(19) zum Buschenfelde, D. M.; Staib, A. *Chem. Phys.* **1998**, *236*, 253.
(20) Veldhuizen, R.; de Leeuw, S. W. *J. Chem. Phys.* **1996**, *105*, 2828.
(21) Staib, A. *J. Chem. Phys.* **1998**, *108*, 4554.
(22) Symons, M. C. R.; Thomas, V. K. *J. Chem. Soc., Faraday Trans. 1* **1981**, *77*, 1883.
(23) Kristiansson, O. *J. Mol. Struct.* **1999**, *477*, 105.
(24) Bertie, J. E.; Zhang, S. L. *J. Mol. Struct.* **1997**, *413−414*, 333.

(25) Asbury, J. B.; Steinel, T.; Stromberg, C.; Gaffney, K. J.; Piletic, I. R.; Goun, A.; Fayer, M. D. *Chem. Phys. Lett.* **2003**, *374*, 362.
(26) Asbury, J. B.; Steinel, T.; Stromberg, C.; Gaffney, K. J.; Piletic, I. R.; Goun, A.; Fayer, M. D. *Phys. Rev. Lett.* **2003**, *91*, 237402.
(27) Asbury, J. B.; Steinel, T.; Stromberg, C.; Gaffney, K. J.; Piletic, I. R.; Fayer, M. D. *J. Chem. Phys.* **2003**, *119*, 12981.
(28) Asbury, J. B.; Steinel, T.; Stromberg, C.; Corcelli, S. A.; Lawrence, C. P.; Skinner, J. L.; Fayer, M. D. *J. Phys. Chem. A* **2004**, *108*, 1107.
(29) Asbury, J. B.; Steinel, T.; Fayer, M. D. *J. Lumin.* **2004**, in press.
(30) Piletic, I. R.; Gaffney, K. J.; Fayer, M. D. *J. Chem. Phys.* **2003**, *119*, 423.
(31) Stenger, J.; Madsen, D.; Hamm, P.; Nibbering, E. T. J.; Elsaesser, T. *J. Phys. Chem. A* **2002**, *106*, 2341.
(32) Stenger, J.; Madsen, D.; Hamm, P.; Nibbering, E. T. J.; Elsaesser, T. *Phys. Rev. Lett.* **2001**, *87*, 027401.
(33) Woutersen, S.; Bakker, H. J. *Phys. Rev. Lett.* **1999**, *83*, 2077.
(34) Gaffney, K. J.; Davis, P. H.; Piletic, I. R.; Levinger, N. E.; Fayer, M. D. *J. Phys. Chem. A* **2002**, *106*, 12012.
(35) Gaffney, K.; Piletic, I.; Fayer, M. D. *J. Phys. Chem. A* **2002**, *106*, 9428.
(36) Gaffney, K. J.; Piletic, I. R.; Fayer, M. D. *J. Chem. Phys.* **2003**, *118*, 2270.
(37) Yeremenko, S.; Pshenichnikov, M. S.; Wiersma, D. A. *Chem. Phys. Lett.* **2003**, *369*, 107.
(38) Fecko, C. J.; Eaves, J. D.; Loparo, J. J.; Tokmakoff, A.; Geissler, P. L. *Science* **2003**, *301*, 1698.
(39) Graener, H.; Ye, T. Q.; Laubereau, A. *J. Chem. Phys.* **1989**, *90*, 3413.
(40) Laenen, R.; Rauscher, C.; Laubereau, A. *J. Phys. Chem. A* **1997**, *101*, 3201.
(41) Laenen, R.; Rausch, C.; Laubereau, A. *Phys. Rev. Lett.* **1998**, *80*, 2622.
(42) Laenen, R.; Gale, G. M.; Lascoux, N. *J. Phys. Chem. A* **1999**, *103*, 10708.
(43) Bratos, S.; Gale, G. M.; Gallot, G.; Hache, F.; Lascoux, N.; Leicknam, J. C. *Phys. Rev. E* **2000**, *61*, 5211.
(44) Bakker, H. J.; Neinhuys, H. K.; Gallot, G.; Lascoux, N.; Gale, G. M.; Leicknam, J. C.; Bratos, S. *J. Chem. Phys.* **2002**, *116*, 2592.
(45) Kropman, M. F.; Nienhuys, H.-K.; Woutersen, S.; Bakker, H. J. *J. Phys. Chem. A* **2001**, *105*, 4622.
(46) Nienhuys, H.-K.; Woutersen, S.; van Santen, R. A.; Bakker, H. J. *J. Chem. Phys.* **1999**, *111*, 1494.
(47) Woutersen, S.; Emmerichs, U.; Bakker, H. J. *J. Chem. Phys.* **1997**, *107*, 1483.
(48) Zimdars, D.; Tokmakoff, A.; Chen, S.; Greenfield, S. R.; Fayer, M. D.; Smith, T. I.; Schwettman, H. A. *Phys. Rev. Lett.* **1993**, *70*, 2718.
(49) Tokmakoff, A.; Fayer, M. D. *J. Chem. Phys.* **1995**, *103*, 2810.
(50) Rector, K. D.; Engholm, J. R.; Rella, C. W.; Hill, J. R.; Dlott, D. D.; Fayer, M. D. *J. Phys. Chem. A* **1999**, *103*, 2381.
(51) Merchant, K. A.; Thompson, D. E.; Fayer, M. D. *Phys. Rev. Lett.* **2001**, *86*, 3899.
(52) Merchant, K. A.; Thompson, D. E.; Xu, Q.-H.; Williams, R. B.; Loring, R. F.; Fayer, M. D. *Biophys. J.* **2002**, *82*, 3277.
(53) Hamm, P.; Lim, M.; Hochstrasser, R. M. *Phys. Rev. Lett.* **1998**, *81*, 5326.
(54) Zanni, M. T.; Asplund, M. C.; Hochstrasser, R. M. *J. Chem. Phys.* **2001**, *114*, 4579.
(55) Golonzka, O.; Khalil, M.; Demirdoven, N.; Tokmakoff, A. *Phys. Rev. Lett.* **2001**, *86*, 2154.
(56) Tanimura, Y.; Mukamel, S. *J. Chem. Phys.* **1993**, *99*, 9496.
(57) Zhang, W. M.; Chernyak, V.; Mukamel, S. *J. Chem. Phys.* **1999**, *110*, 5011.
(58) Mukamel, S. *Annu. Rev. Phys. Chem.* **2000**, *51*, 691.
(59) Venkatramani, R.; Mukamel, S. *J. Chem. Phys.* **2002**, *117*, 11089.
(60) Ernst, R. R.; Bodenhausen, G.; Wokaun, A. *Nuclear Magnetic Resonance in One and Two Dimensions*; Oxford University Press: Oxford, U.K., 1987.
(61) Berg, M.; Walsh, C. A.; Narasimhan, L. R.; Littau, K. A.; Fayer, M. D. *J. Chem. Phys.* **1988**, *88*, 1564.
(62) Littau, K. A.; Bai, Y. S.; Fayer, M. D. *Chem. Phys. Lett.* **1989**, *159*, 1.
(63) Tokmakoff, A.; Urdahl, R. S.; Zimdars, D.; Kwok, A. S.; Francis, R. S.; Fayer, M. D. *J. Chem. Phys.* **1995**, *102*, 3919.
(64) Berg, M. A.; Rector, K. D.; Fayer, M. D. *J. Chem. Phys.* **2000**, *113*, 3233.
(65) Tokmakoff, A. *J. Phys. Chem. A* **2000**, *104*, 4247.
(66) Hybl, J. D.; Christophe, Y.; Jonas, D. M. *Chem. Phys.* **2001**, *266*, 295.
(67) Iwaki, L. K.; Dlott, D. D. *J. Phys. Chem. A* **2000**, *104*, 9101.
(68) Khalil, M.; Demirdoven, N.; Tokmakoff, A. *J. Phys. Chem. A* **2003**, *107*, 5258.
(69) Khalil, M.; Demirdoven, N.; Tokmakoff, A. *Phys. Rev. Lett.* **2003**, *90*, 047401(4).
(70) Hybl, J. D.; Ferro, A. A.; Jonas, D. M. *J. Chem. Phys.* **2001**, *115*, 6606.
(71) Levinger, N. E.; Davis, P. H.; Fayer, M. D. *J. Chem. Phys.* **2001**, *115*, 9352.
(72) Mukamel, S. *Principles of Nonlinear Optical Spectroscopy*; Oxford University Press: New York, 1995.
(73) Asbury, J. B.; Steinel, T.; Fayer, M. D. *Chem. Phys. Lett.* **2003**, *381*, 139.
(74) Morita, H. N., Saburo. *J. Mol. Spectrosc.* **1974**, *49*, 401.
(75) Luzar, A. *J. Chem. Phys.* **2000**, *113*, 10663.
(76) Bertolini, D.; Cassettari, M.; Ferrario, M.; Grigolini, P.; Salvetti, G. *Adv. Chem. Phys.* **1985**, *62*, 277.